Hindawi
Geofluids
Volume 2022, Article ID 9822469, 11 pages
https://doi.org/10.1155/2022/9822469

Research Article

Investigation on Energy Evolution and Storage Characteristic of CSTBD Red Sandstone during Mixed-Mode Fracture

Wuxing Wu [1,2] and Fengqiang Gong [1,2]

[1] *Engineering Research Center of Safety and Protection of Explosion & Impact of Ministry of Education (ERCSPEIME), Southeast University, Nanjing 211189, China*
[2] *School of Civil Engineering, Southeast University, Nanjing 211189, China*

Correspondence should be addressed to Fengqiang Gong; fengqiangg@126.com

Received 12 June 2022; Accepted 1 October 2022; Published 17 October 2022

Academic Editor: Mohammed Fattah

To investigate the energy evolution and storage characteristics of the rock during the mixed-mode fracture failure, several single loading-unloading tests under preset different unloading levels were conducted on the cracked straight-through Brazilian disc (CSTBD) red-sandstone specimen with crack inclination angles of 10° and 20°. The input energy, elastic energy, and dissipated energy parameters were obtained by calculating the area integral of the load-displacement curve. Test results display that the total input energy, elastic energy, and dissipated energy of rock specimens increase in quadratic function with the increase of unloading level at different unloading levels. It was found that there are significant linear energy storage and dissipation laws of rock during the mixed-mode fracture process. The concepts of fracture energy storage coefficient (FESC) and fracture energy dissipation coefficient (FEDC) were proposed to express the energy variation of rock in the prepeak stage. Under the same loading conditions, FESC and FEDC remain unchanged regardless of crack inclination angles, indicating that the linear energy storage and dissipation laws are an inherent property of the rock. Besides, the peak fracture elastic-dissipation index W_{ed} (the ratio of peak elastic energy to peak dissipation energy) was obtained through quantitative analysis and demonstrated its invariant feature.

1. Introduction

In deep underground engineering, the surrounding rock often induces fracture failure [1–4], and the mixed-mode fracture failure mode is often dominant due to the influence of its various flaw defects [5–8]. In recent decades, many research scholars have developed and reported different loading devices and various specimens which are precracked to investigate the mechanism of rock mixed-mode fracture. Some well-known test methods are cracked straight through Brazilian disc (CSTBD) under diametral compression [9, 10], compact-tension-shear [11, 12], three-point bending [13, 14], four-point bending [15, 16], and angled internal cracked plate [17, 18]. Among these test methods, the CSTBD specimen can carry out multiple forms of mixed-mode fracture tests by rotating the orientation of the central crack (i.e., crack inclination angle α) relative to the loading direction and altering the crack length, which has been widely considered as the preferred test specimen for mixed-mode fracture on rocks. For example, Ayatollahi and Aliha [10] conducted mixed-mode fracture tests using CSTBD specimens, and the experimental results conform to the generalized maximum tensile stress criterion. By the advantages of CSTBD, many scholars have made some significant achievements in the study of rock mixed-mode fracture. Therefore, CSTBD specimens are also used for the mixed-mode fracture test in this study.

So far, studying the rock mass failure mechanisms from the energy perspective has received more and more attention from engineering and theoretical circles [19]. For example, Gong et al. [20] proposed the linear energy storage law for the first time by conducting a single loading-unloading test on 14 kinds of rocks under uniaxial compression and established the rockburst proneness criterion of the residual elastic energy index, which greatly promoted the understanding of energy evolution in the rock failure process. Zhang [21] conducted a conventional impact test on the Brazilian disk of red sandstone and found that the kinetic energy released during rock fracture is very significant and increases with the increase of loading rate. Wang et al. [22] explored the characteristics of energy evolution during rock failure at different bedding angles under uniaxial compression. Moreover, Zhang and Ouchterlony [23] systematically summarized the energy requirement for rock failure from laboratory tests and field operations based on the review of a wide range of literature. Yang et al. [24] conducted a series of uniaxial compression tests on the Silurian Longmaxi shale specimens and, combined with Griffith's theory of crack propagation, established a theoretical framework for energy conversion and distribution during hard rock failure. Meng et al. [25] studied the energy accumulation, evolution, and dissipation characteristics of 30 sandstone specimens during uniaxial cyclic loading and unloading compression at six different loading rates and found that the energy parameters of rock specimens increase nonlinearly with increasing axial loading stress. Chen et al. [26] used the modified true triaxial rockburst test system to conduct rockburst tests on rectangular prismatic coarse-grained granite under different loading rates and found that with the loading rate increasing from 0.5 to 4.0 MPa/s, the fragmentation and energy dissipation of fragments decreased linearly. Bagde and Petoroš [27] conducted uniaxial cyclic compression tests on rocks with different frequencies and amplitudes and found that the dynamic energy sustained by the rock showed an increasing trend with frequency and amplitude. Gong et al. [28] used red sandstone three-point bending specimens to study the energy evolution characteristics during the mode I fracture process and found that the elastic energy and input energy, dissipated energy, and input energy have a strong linear relationship during the fracture failure process. Luo and Gong [29] used the three-point loading technique to carry out a series of single-cycle loading and unloading flexural fracture tests on rectangular rock beams and found that under different experimental unloading levels, the elastic and dissipation energies increase linearly as the input energy increases. It is well-known that rocks often have mixed-mode fracture failure characteristics, and the study of the energy evolution characteristics in the process of mixed-mode fracture failure is also of great significance to understand the rock failure mechanism.

The mixed-mode fracture test can be achieved by rotating the inclination of the crack in the CSTBD specimen to the loading direction [10]. Thus, the CSTBD specimens with crack inclination angles of 10° and 20° under diametral compression were used to study the energy evolution during mixed-mode fracture. It is divided into the sustained loading mixed-mode fracture test (SLMF) and the single loading-unloading mixed-mode fracture test (SLUMF), wherein the initial peak fracture load of the SLMF tests provides a reference for the design of the unloading level in SLUMF tests. Based on the load-displacement curve obtained from SLUMF tests, the energy parameters including input energy, elastic energy, and dissipated energy were visualized by the area integral method. Test results reveal that there is an obvious strong linear relationship between elastic energy, dissipated energy, and input energy. Simultaneously, the constant characteristics of the peak fracture elastic-dissipation index W_{ed} were obtained through quantitative analysis. From the point of view of energy, the evolution characteristics of energy storage and energy dissipation in the process of rock mixed-mode fracture were analyzed and discussed in detail.

2. Test Preparation

2.1. Rock Material Characteristics. The red sandstone specimens were selected for this test due to their good homogeneity. Figure 1 shows the internal microstructure and corresponding mineral composition of red sandstone. The description of its mineral composition was detailed in reference [30]. Before the tests, the red sandstone was subjected to uniaxial compression, Brazilian splitting, and other tests to obtain the following basic physical and mechanical parameters: average uniaxial compressive strength $\sigma_c = 97.5$ MPa, average indirect tensile strength $\sigma_t = 4.87$ MPa, average density $\rho = 2430.18\,\mathrm{kg/m^3}$, and average P-wave $V = 3.01$ km/s. In addition, Gong et al. [20] judged that the red sandstone has a moderate rockburst proneness based on the residual elastic energy index.

For the rock specimen preparation of the mixed-mode fracture test, the red sandstone was processed into the standard CSTBD specimens. The CSTBD specimen with a diameter $2R = 50$ mm and thickness $t = 25$ mm, and the crack with length $l = 25$ mm and width $w = 1$ mm (as shown in Figure 2). The mixed-mode fracture test can be achieved by rotating the inclination of the crack in the CSTBD specimen to the loading direction, i.e., angle α. The MTS Insight-23 electromechanical testing system was used to obtain the load-displacement deformation curve of the specimens (Figure 2). During the test, the CSTBD specimens were placed in the test equipment by rotating it around the centerline by $\alpha = 10°$ or $\alpha = 20°$, respectively.

2.2. Experiment Procedure. For each specimen group ($\alpha = 10°$ and $\alpha = 20°$), including the SLMF tests and SLUMF tests, the SLMF test refers to loading the specimen at a constant loading rate (2 kN/min) until failure occurs, to obtain the initial peak fracture load values (F^i_{peak}) of the specimens CSTBD-10° and CSTBD-20°, as shown in Figure 3(a). The SLUMF test means that the testing machine was first loaded to a preset load, and then, the unloading operation was performed; after the unloading is completed, the second loading is performed until the rock failure. Based on the initial peak load, five single loading-unloading tests with different unloading levels were set up, where the unloading levels (i) were approximately 0.1, 0.3, 0.5, 0.7, and 0.9 of the initial peak fracture loads, respectively, as shown in Figure 3(b). Observe that in the SLUMF test, the unloading curve was not unloaded to 0 kN but 0.02 F^i_{peak}, which was to prevent separation between the specimen and the equipment. This does not affect the test results, which has been confirmed by our previous research [20].

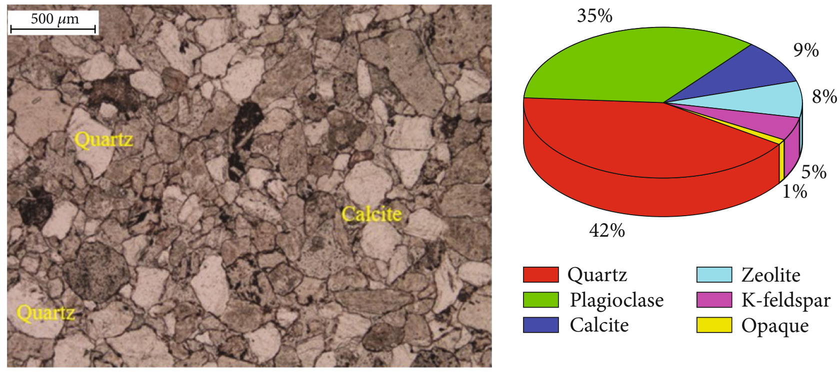

FIGURE 1: Red-sandstone mineral composition [30].

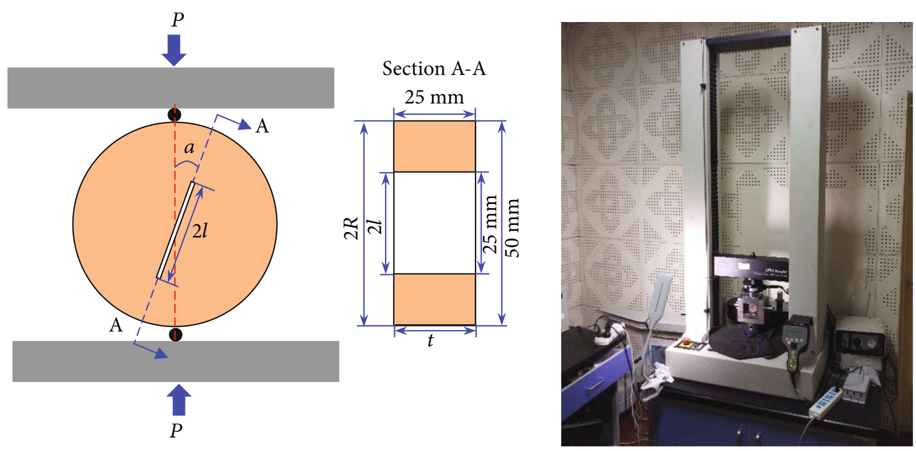

FIGURE 2: CSTBD red sandstone specimen.

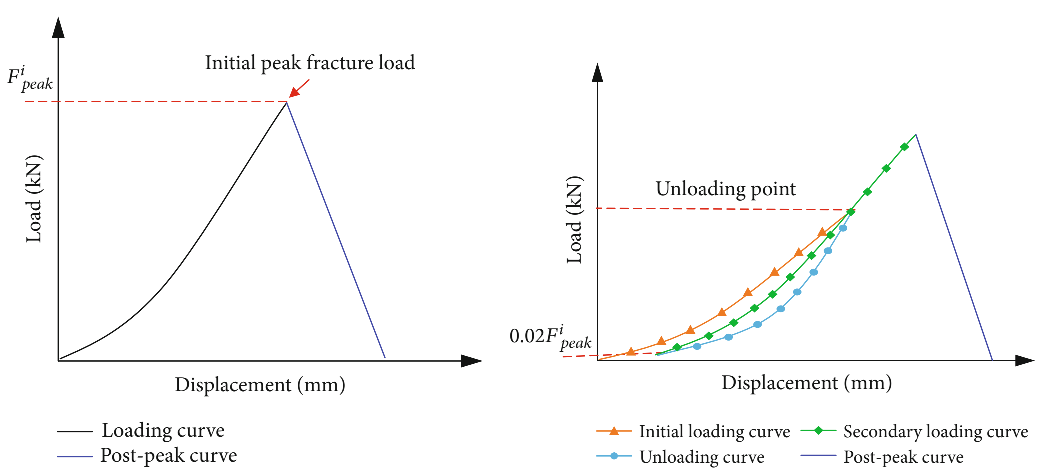

(a) (b)

FIGURE 3: Load-displacement diagram of stress path: (a) SLMF test; (b) SLUMF test.

3. Load-Displacement Responses

3.1. SLMF Test. Figure 4 illustrates the load-displacement curves of $\alpha = 10^\circ$ and $\alpha = 20^\circ$ under the SLMF test. For the $\alpha = 10^\circ$ group, the mixed-mode fracture load values are 4.86, 5.06, and 4.70 kN, respectively; the initial peak fracture load values are 4.87 kN; and the peak fracture displacements are 0.28, 0.26, and 0.22 mm, respectively (as shown Table 1). For the specimen $\alpha = 20^\circ$ group, the mixed-mode fracture load values are 4.76, 4.95, and 4.93 kN, respectively, and the initial peak fracture load values are 4.88 kN, and the peak fracture displacements are 0.17, 0.17, and 0.22 mm, respectively (as shown Table 1). Additionally, the load-displacement curves under the SLMF condition show the

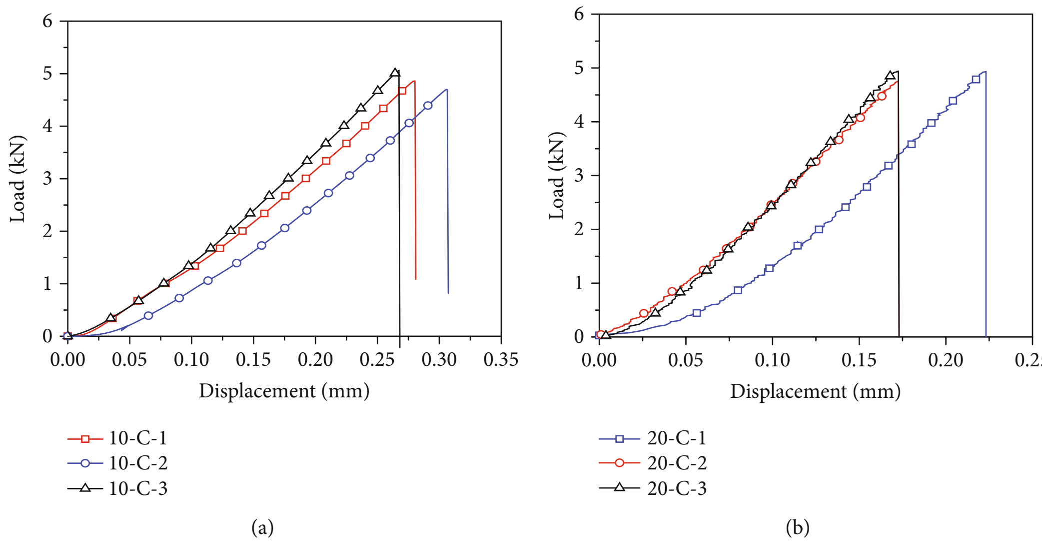

Figure 4: Load-displacement of SLMF tests: (a) $\alpha = 10^{\circ}$; (b) $\alpha = 20^{\circ}$.

Table 1: SLMF test results.

Specimen ID	Peak fracture load (kN)	Average peak fracture load (kN)	Peak fracture displacements (mm)
10-C-1	4.86		0.28
10-C-2	5.06	4.87	0.26
10-C-3	4.70		0.22
20-C-1	4.76		0.17
20-C-2	4.95	4.88	0.17
20-C-3	4.93		0.22

nonlinear rise first and then approximately linear rise characteristics. Taking the initial peak fracture load values as a reference, set the unloading point levels as 0.1 F^i_{peak}, 0.3 F^i_{peak}, 0.5 F^i_{peak}, 0.7 F^i_{peak}, and 0.9 F^i_{peak}. For the $\alpha = 10^{\circ}$ group, the corresponding load values at the unloading point are 0.487, 1.461, 2.435, 3.409, and 4.383 kN, respectively. For the $\alpha = 20^{\circ}$ group, the corresponding load values at the unloading point are 0.488, 1.464, 2.440, 3.416, and 4.392 kN, respectively, as shown in Table 2.

3.2. SLUMF Tests. Following the above test plans, the SLUMF tests with $\alpha = 10^{\circ}$and $\alpha = 20^{\circ}$ were performed on the CSTBD specimens. The typical load-displacement curves of the SLUMF test of the CSTBD specimens are shown in Figure 5. On the whole, the single loading-unloading curve rises nonlinearly before the unloading point, which may be caused by the internal crack compression and propagation of CSTBD specimens; after the unloading point, it rises approximately linearly until the peak fracture load. Moreover, the overall characteristics of the single loading-unloading curves are basically the same as those of the curves under the SLMF conditions (Figure 4). Additionally, the unloading curve and the secondary loading curve at different unloading levels are approximately the same as the initial loading curve. When the secondary loading curve reaches the unloading point, the specimen still can withstand external loads until the failure occurs at the peak load. Furthermore, the load on the initial loading curve is significantly higher than that on the secondary loading curve, and a certain area is formed between the two curves. Therefore, it can be inferred that under the SLUMF condition, there is energy dissipation during the specimen fractured.

4. Energetic Interpretations of Experimental Results and Discussion

4.1. Energy Calculation Principle. Generally, the indicators used to describe the characteristics of energy evolution during rock failure include input energy, internal elastic energy, and dissipated energy [31, 32]. Obtaining the load-displacement curve in the SLUMF tests and performing area integration on it can effectively and accurately obtain the energy evolution parameters during the rock failure process, which has been confirmed by Gong et al. [20]. Figure 6 shows the calculation of the three energy parameters at a certain unloading level by the area integral method. For more information on the calculation and definition of energy parameters in area integration, please refer to reference [20]. Therefore, the total input energy E_{ai}, elastic energy E_{ei}, and dissipation energy E_{di} of the rock material at the unloading level i satisfy the following relations:

$$\begin{cases} E_{ai} = \int_0^{u_2} F\mathrm{d}u, \\ E_{ei} = \int_{u1}^{u_2} F\mathrm{d}u, \\ E_{di} = \int_0^{u_2} F\mathrm{d}u - \int_{u1}^{u_2} F\mathrm{d}u. \end{cases} \tag{1}$$

4.2. The Nonlinear Increasing Energy Tendency during Mixed-Mode Fracture Test. Based on the energy calculation method

Table 2: Test parameters.

α	Specimen ID	Load at preset unloading level (kN)	Preset unloading level	Loading rate
	10-S-1	0.487	0.1	
	10-S-2	1.461	0.3	
10°	10-S-3	2.435	0.5	
	10-S-4	3.409	0.7	
	10-S-5	4.383	0.9	Initial loading and unloading curves: 2 kN/min Secondary loading curve: 0.1 mm/min
	20-S-1	0.488	0.1	
	20-S-2	1.464	0.3	
20°	20-S-3	2.440	0.5	
	20-S-4	3.416	0.7	
	20-S-5	4.392	0.9	

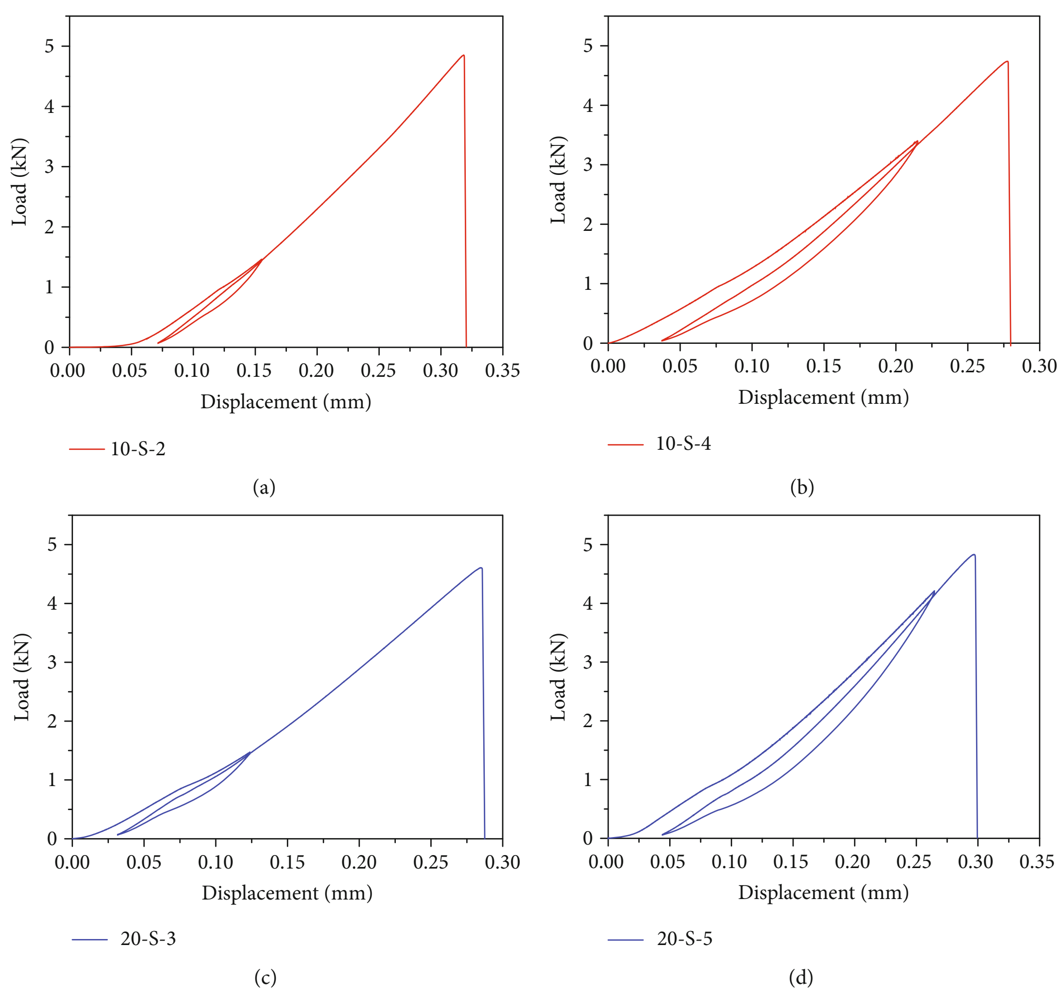

Figure 5: Typical load-displacement of SLUMF tests: (a) specimen 10-S-2; (b) specimen 10-S-4; (c) specimens 20-S-3; (d) specimens 20-S-5.

shown in Figure 6, the E_{ai}, E_{ei}, and E_{di} at the different i under different specimen groups are obtained and shown in Figure 7. Obviously, the energy parameters under different i are different and increase with the increase of i. To further analyze the variations of these energy parameters at different inclination angles with the different unloading levels, the statistical analysis of the dates is shown in Figure 8. As shown, each energy parameter increases nonlinearly with the increase of i, which conforms to the quadratic fitting function. For the $\alpha = 10°$, the quadratic fit coefficients (R^2) between these energy parameters and the unloading level were 0.9987, 0.9979, and 0.9942, respectively, indicating a strong nonlinear relationship. Similarly, the same treatment was performed on the $\alpha = 20°$, and the R^2 was 0.9978, 0.9987, and 0.9901, respectively. The E_{ai}

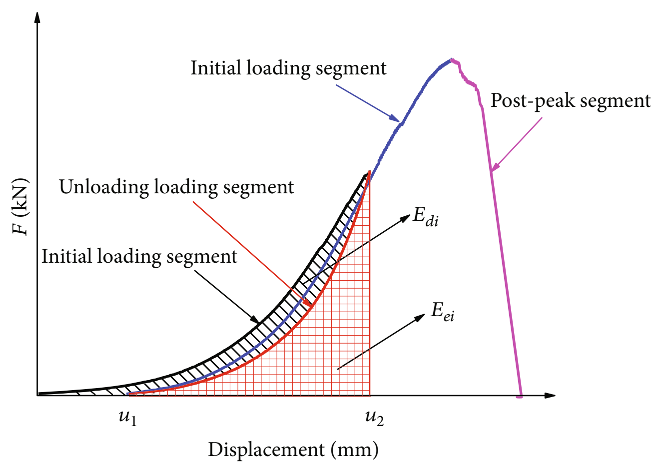

Figure 6: Schematic diagram of energy parameters calculated by area integration method.

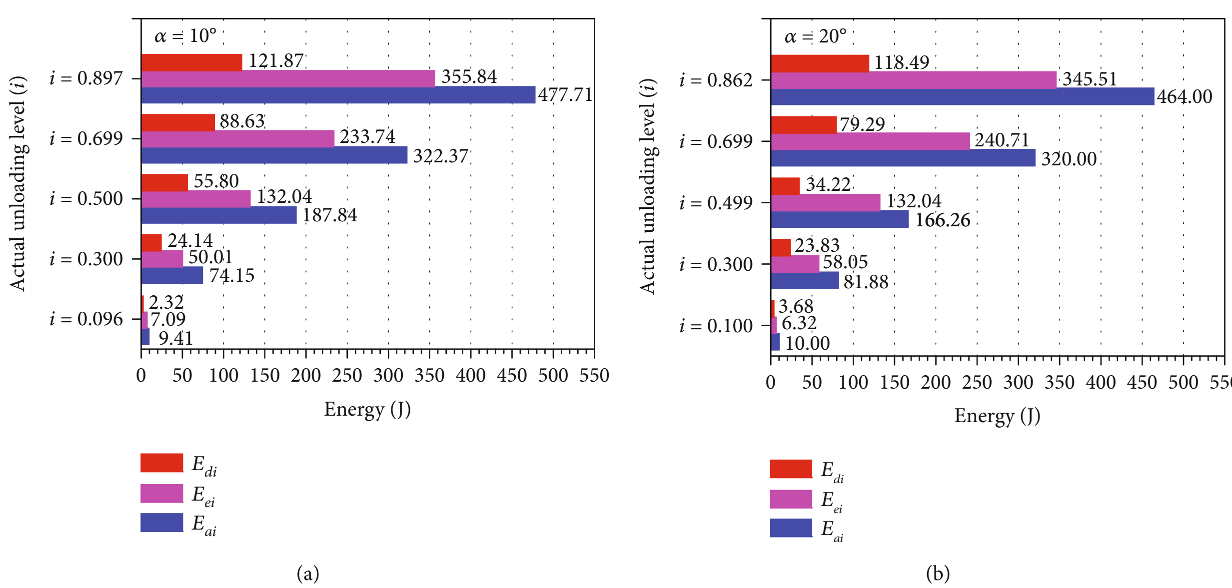

Figure 7: Various energy indicators at different unloading levels: (a) $\alpha = 10^\circ$; (b) $\alpha = 20^\circ$.

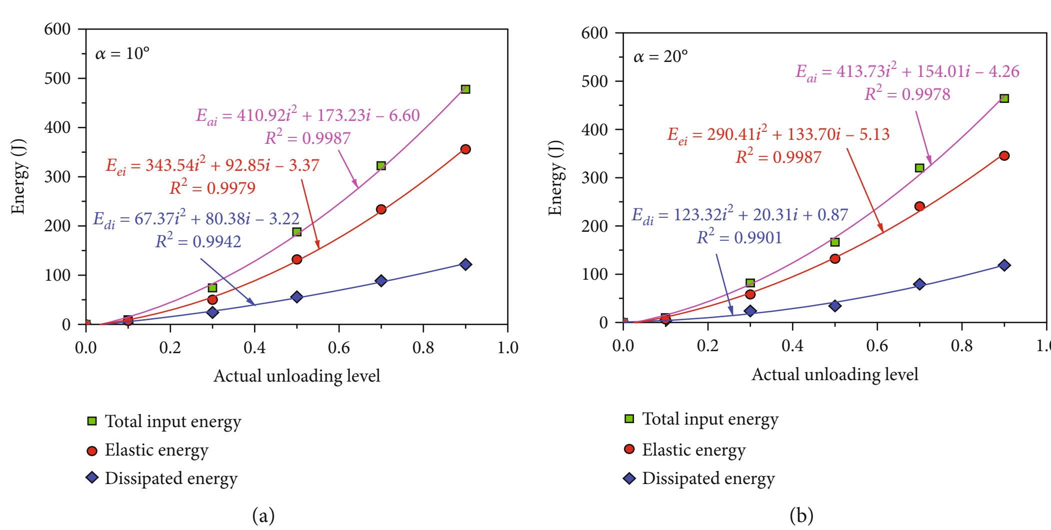

Figure 8: Energy characteristics at the unloading level: (a) $\alpha = 10^\circ$; (b) $\alpha = 20^\circ$.

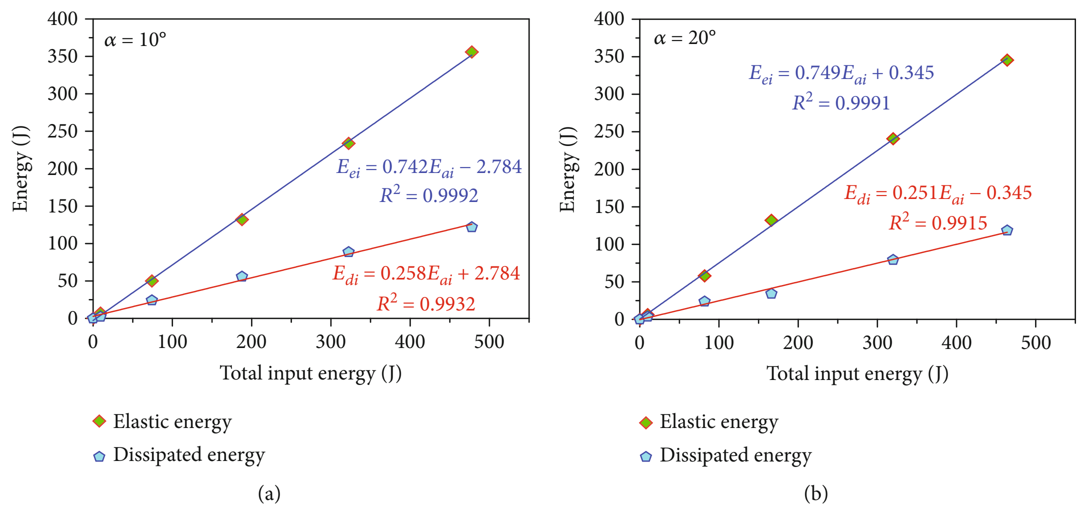

FIGURE 9: Linear relationship of energy: (a) $\alpha = 10^{\circ}$; (b) $\alpha = 20^{\circ}$.

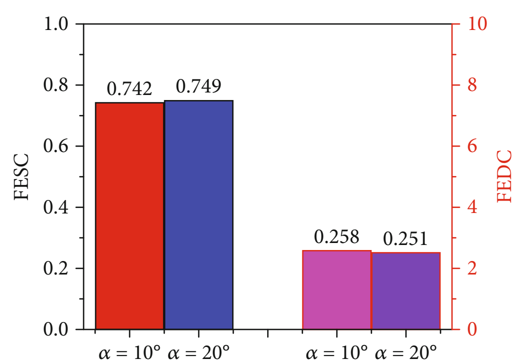

FIGURE 10: Illustration of FESC and FEDC results.

was always the largest and followed by E_{ei} and then E_{di} regardless of the i. Moreover, the gap between the E_{ai} and the E_{ei} was significantly smaller than the gap between the E_{ei} and the E_{di}, and the difference between the two gaps increases gradually with the increases of the i. Furthermore, the increase rate of E_{ei} is much greater than that of E_{di} as the i increases, which indicates that a large amount of elastic energy will be stored in the hard rock when subjected to higher unloading levels. These results were essentially the same for both $\alpha = 10\circ$ and $\alpha = 20^{\circ}$.

4.3. The Linear Energy Storage and Dissipation Laws during Mixed-Mode Fracture Test. To further understand the relationship between the various energies of the rock during the mixed-mode fracture process, the E_{ai} was taken as the horizontal ordinate to investigate the relationship between E_{ei} and E_{ai} and E_{di} and E_{ai}, as shown in Figure 9. Interestingly, the E_{ei} and E_{ai} and E_{di} and E_{ai} of the $\alpha = 10^{\circ}$ and $\alpha = 20^{\circ}$ follow the linear function of one variable relationship. Based on this, the linear relationship between E_{ei} and E_{ai} and E_{di} and E_{ai} is defined as linear energy storage law (LESL) and linear energy dissipation law (LEDL), respectively. Gong et al. [20] first found the LESL and LEDL in uniaxial compressed rocks. Moreover, LESL and LEDL exist not only in the rock compression test but also in the loading process of coal and concrete [33, 34]. Thus, the LESL and LEDL can be defined as

$$\begin{cases} E_{ei} = aE_{ai} - c, \\ E_{di} = bE_{ai} + c, \\ 1 = a + b, \end{cases} \tag{2}$$

where a and b are referred to as the energy storage coefficient and energy dissipation coefficient, respectively, and c is the fitting parameter.

Furthermore, the FESC and FEDC are defined as the fracture energy storage coefficient and fracture energy dissipation coefficient, respectively, to characterize the energy conversion relationship within the rock in the prepeak stage. Based on the LESL and LEDL, the FESC and FEDC correspond to slopes a and b, respectively. So, the FESC and FEDC can reflect the ability of energy storage and dissipation in the rock fracture failure process. Notably, the sum of FESC and FEDC equals 1 and is not affected by α. This shows that in the rock fracture process, the E_{ai} is converted into E_{ei} and E_{di} in proportion. No matter how the crack inclination changes, the LESL and LEDL are always established (Figure 9), which also indicates that the LESL and LEDL are inherent properties of the rock itself. As illustrated in Figure 10, the FESC and FEDC of the $\alpha = 10^{\circ}$ and $\alpha = 20^{\circ}$ are very close, and the specific values of FESC and FEDC are 0.742 and 0.258, 0.749, and 0.251, respectively. The maximum difference between the two FESC is 0.007, the difference between FEDC is 0.007, and the difference is very small and can be ignored. This further shows that the crack inclination angle does not affect the energy conversion ratio. In other words, the energy conversion ratio of the input energy to the elastic energy and the dissipated energy is constant in the mixed-mode fracture test. In conclusion, these results demonstrate that the LESL, LEDL, and the corresponding energy conversion ratio are the inherent properties of rock materials in the mixed-mod fracture process.

Table 3: Basic physical mechanical and energy parameters.

α	Specimen ID	ρ (g/mm^3)	V (km/s)	F_{max} (kN)	U_p (mm)	E_a (J)	E_e (J)	E_d (J)	W_{ed} (J)
	10-S-1	2359.385	3.101	0.278	4.640	563.79	420.73	143.06	2.941
	10-S-2	2377.776	2.956	0.319	4.850	591.46	441.40	150.06	2.941
10°	10-S-3	2363.182	3.001	0.310	4.600	568.36	424.14	144.22	2.940
	10-S-4	2368.277	3.008	0.278	4.740	518.50	386.90	131.60	2.940
	10-S-5	2682.261	2.987	0.279	4.760	627.36	468.13	159.23	2.940
	20-S-1	2509.458	2.990	0.298	4.630	563.81	422.25	141.56	2.983
	20-S-2	2611.053	2.980	0.285	4.610	583.82	437.22	146.60	2.982
20°	20-S-3	2360.333	3.010	0.249	4.380	515.65	386.22	129.42	2.984
	20-S-4	2372.067	2.899	0.275	4.590	594.67	445.34	149.33	2.982
	20-S-5	2351.829	3.009	0.297	4.830	675.46	505.77	169.69	2.981

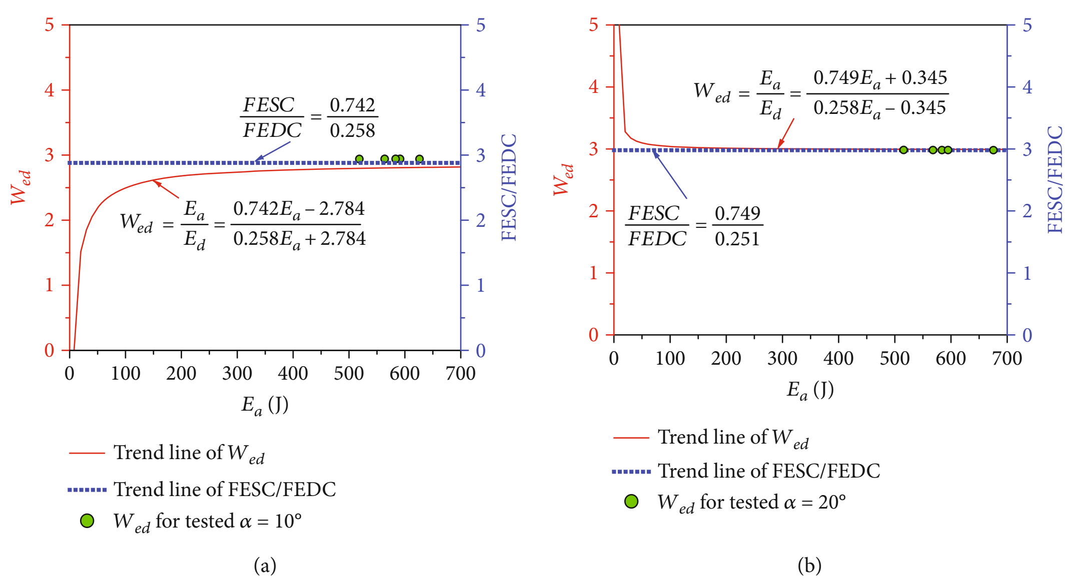

Figure 11: Variation in W_{ed} for the red sandstone.

4.4. The Invariable Feature of W_{ed} in Mixed-Mod Fracture Process. Generally, the energy accumulated by the rock specimen has reached its limit before reaching its critical failure point (i.e., peak load point). Thus, it is very necessary to understand the energy conversion characteristics at the peak load point. Gong et al. [20] first founded the LESL and LEDL and extended them to calculate peak input energy E_a, peak elastic energy E_e, and the peak dissipation energy E_d at the peak load point, and this method has been generally recognized. So, the specific calculation process of each energy parameter at the peak load point can be found in our literature [20]. Thus, this study calculates the E_a, E_e, and E_d at the peak fracture load point during the mixed-mod fracture process according to the same logical relationship, as follows:

$$\begin{cases} E_e = aE_a - c, \\ E_d = bE_a + c, \\ 1 = a + b. \end{cases} \tag{3}$$

Table 3 gives the detailed calculations of E_a, E_e, and E_d. To better characterize the energy conversion relationship of rock fracture failure at the peak fracture load point, the ratio of E_e/E_d (which can be named as peak fracture elastic-dissipation index W_{ed}) was proposed to be expressed:

$$W_{ed} = \frac{E_e}{E_d} = \frac{aE_a - c}{bE_a + c}. \tag{4}$$

Figure 11 plots the W_{ed} trend line and the ratio of FESC/FEDC. It can be seen that theW_{ed}initially fluctuates greatly at the$E_a$which is low, and the W_{ed} gradually tends to converge to a constant value as the E_a exceeds a certain value. Furthermore, the larger the E_a, the W_{ed} basically converges to the constant FESC/FEDC.

It is well-known that basic physical and mechanical parameters such as rock density, longitudinal wave velocity, and elastic modulus are characterized as inherent properties of rock. Based on the above analysis, W_{ed} eventually tends to a constant value, which may be considered the inherent

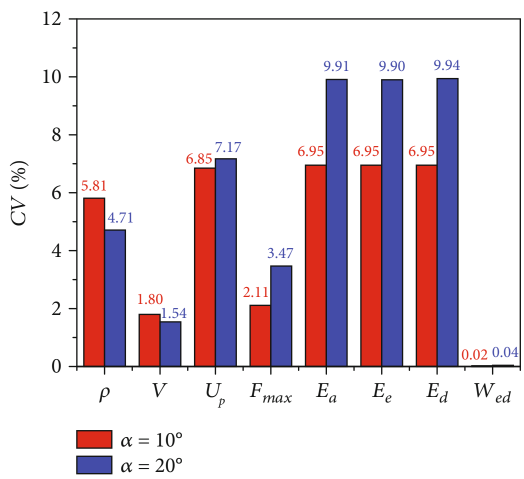

Figure 12: Illustration of CV values.

characteristics of the rock. Thus, we analyze some basic mechanical and energy parameters such as density (ρ), wave velocity (V), peak load ($F_{\max}$), peak displacement (U_{p}), E_{a}, E_{e}, and E_{d} for each specimen (as shown in Table 3) and quantify the deviation of these parameters for each specimen using the coefficient variation (CV) and compared with W_{ed}. The coefficient of variation is a dimensionless coefficient used to compare the degree of dispersion of multiple sets of data, and it is defined as follows [35]:

$$\mathrm{CV}=\frac{\sqrt{(1/(n-1))\sum_1^n\left(X-(1/(n-1))\sum_1^n X\right)^2}}{(1/n)\sum_1^n X}, \quad (5)$$

where n is the amount of data in the same attribute group and X represents different attribute groups.

Figure 12 shows the CV values corresponding to the basic physical mechanical and energy parameters of each group of specimens. Whether the $\alpha=10^\circ$ or $\alpha=20^\circ$, the E_{a}, E_{e}, and E_{d} of the specimen all show high CV values (6.95~9.94%); that is, these energy parameters show serious dispersion. Even the $F_{\max}$ and U_{p} of the specimen showed obvious dispersion, and the CV value also fluctuated in the range of 2.11~7.17%. Compared with other parameters occupying such a high CV value, the parameter W_{ed} shows an extremely small CV value and is not affected by the α. The CV values of W_{ed} for sandstone specimen under the $\alpha=10^\circ$ and $\alpha=20^\circ$ are 0.02% and 0.04%, respectively. The above contrasting arguments strongly confirm that W_{ed} can be regarded as an inherent property of rocks. Besides, the W_{ed} also intuitively represents that the energy distribution of elastic energy and dissipated energy at the peak point of rock is fixed, which is the inherent property of rock. Moreover, W_{ed} can be used as an inherent index, which has also been confirmed in compression and three-point bending tests [29, 36].

5. Conclusions

In this paper, two types of crack inclination angle ($\alpha=10^\circ$ and $\alpha=20^\circ$) CSTBD specimens were used for single loading-unloading mixed fracture tests, and the energy evolution characteristics were analyzed. The following conclusions were obtained:

(1) During the mixed-mode fracture process, the $E_{\mathrm{a}i}$, $E_{\mathrm{e}i}$, and $E_{\mathrm{d}i}$ have a nonlinear relationship with the i and highly follow the quadratic nonlinear function. With the increase of the i, the growth rate of the $E_{\mathrm{a}i}$ is the largest, followed by the $E_{\mathrm{e}i}$, and finally the $E_{\mathrm{d}i}$

(2) It was found that there are significant LESL and LEDL of rock during the mixed-mode fracture process. Further, the FESC and FEDC were proposed to express the energy variation of rock in the prepeak stage. Under the same loading conditions, FESC and FEDC remain unchanged regardless of crack inclination angles, indicating that the LESL and LEDL are inherent properties of the rock

(3) Based on the LESL and LEDL, the E_{a}, E_{e}, and E_{d} throughout the prepeak loading stage are quantitatively determined. The peak fracture elastic-dissipation index W_{ed} was introduced and demonstrated its invariant feature. Further, by comparing the CV values of other basic physical and mechanical parameters of the rock specimen, it is confirmed that W_{ed} can be regarded as a physical parameter of rock material that reflects the inherent energy characteristics at the peak point

Data Availability

All data generated or analyzed during this study are included in this published article.

Conflicts of Interest

The authors declare that they have no conflicts of interest.

Acknowledgments

This work was supported by the National Natural Science Foundation of China (Grant No. 42077244) and the Fundamental Research Funds for the Central Universities (Grant No. 2242022k30054). Many thanks are due to Jifu Gao, the general manager of Jing Cheng Geotechnical Service Company which locates in Liuyang City, Hunan Province of China, for his sincere help in processing rock specimens.

References

[1] Q. B. Zhang and J. Zhao, “Effect of loading rate on fracture toughness and failure micromechanisms in marble,” *Engineering Fracture Mechanics*, vol. 102, pp. 288–309, 2013.

[2] Q. H. Rao, Z. Q. Sun, G. Y. Wang, J. C. Xu, and J. Y. Zhang, “Effect of specimen thickness on mode II fracture toughness of rock,” *Journal of Central South University*, vol. 8, no. 2, pp. 114–119, 2001.

[3] P. Y. Asem, X. R. Wang, C. Hu, and J. F. Labuz, "On tensile fracture of a brittle rock," *International Journal of Rock Mechanics and Mining Sciences*, vol. 144, p. 104823, 2021.

[4] C. Zhu, M. Karakus, M. C. He et al., "Volumetric deformation and damage evolution of Tibet interbedded skarn under multistage constant-amplitude-cyclic loading," *International Journal of Rock Mechanics and Mining Sciences*, vol. 152, p. 105066, 2022.

[5] N. A. Al-Shayea, "Crack propagation trajectories for rocks under mixed mode I-II fracture," *Engineering Geology*, vol. 81, no. 1, pp. 84–97, 2005.

[6] Z. L. Ru, H. B. Zhao, and S. D. Yin, "Evaluation of mixed-mode stress intensity factors by extended finite element method," *Journal of Central South University*, vol. 20, no. 5, pp. 1420–1425, 2013.

[7] X. P. Zhou, J. Bi, and Q. H. Qian, "Numerical simulation of crack growth and coalescence in rock-like materials containing multiple pre-existing flaws," *Rock Mechanics and Rock Engineering*, vol. 48, no. 3, pp. 1097–1114, 2015.

[8] L. Lang, Z. M. Zhu, H. B. Wang, J. W. Huang, M. Wang, and X. S. Zhang, "Effect of loading rates on crack propagating speed, fracture toughness and energy release rate using single-cleavage trapezoidal open specimen under impact loads," *Journal of Central South University*, vol. 27, no. 8, pp. 2440–2454, 2020.

[9] K. Khan and N. A. Al-Shayea, "Effect of specimen geometry and testing method on mixed I–II fracture toughness of a limestone rock from Saudi Arabia," *Rock Mechanics and Rock Engineering*, vol. 33, no. 3, pp. 179–206, 2000.

[10] M. R. Ayatollahi and M. R. M. Aliha, "On the use of Brazilian disc specimen for calculating mixed mode I-II fracture toughness of rock materials," *Engineering Fracture Mechanics*, vol. 75, no. 16, pp. 4631–4641, 2008.

[11] H. F. Azar, N. Choupani, H. Afshin, and R. H. Moghadam, "Effect of mineral admixtures on the mixed-mode (I/II) fracture characterization of cement mortar: CTS, CSTBD and SCB specimens," *Engineering Fracture Mechanics*, vol. 134, pp. 20–34, 2015.

[12] H. A. Richard and K. Benitz, "A loading device for the creation of mixed mode in fracture mechanics," *International Journal of Fracture*, vol. 22, no. 2, pp. R55–R58, 1983.

[13] M. R. Ayatollahi, M. R. M. Aliha, and H. Saghafi, "An improved semi-circular bend specimen for investigating mixed mode brittle fracture," *Engineering Fracture Mechanics*, vol. 78, no. 1, pp. 110–123, 2011.

[14] M. R. M. Aliha, G. R. Hosseinpour, and M. R. Ayatollahi, "Application of cracked triangular specimen subjected to three-point bending for investigating fracture behavior of rock materials," *Rock Mechanics and Rock Engineering*, vol. 46, no. 5, pp. 1023–1034, 2013.

[15] L. Marsavina, T. Sadowski, and M. Knec, "Crack propagation paths in four point bend aluminium-PMMA specimens," *Engineering Fracture Mechanics*, vol. 108, pp. 139–151, 2013.

[16] S. M. J. Razavi, M. R. M. Aliha, and F. Berto, "Application of an average strain energy density criterion to obtain the mixed mode fracture load of granite rock tested with the cracked asymmetric four- point bend specimens," *Theoretical and Applied Fracture Mechanics*, vol. 97, pp. 419–425, 2018.

[17] J. G. Williams and P. D. Ewing, "Fracture under complex stress–the angled crack problem," *International Journal of Fracture Mechanics*, vol. 8, no. 4, pp. 441–446, 1972.

[18] U. Yukio, I. Kazuo, Y. Tetsuya, and A. Mitsuru, "Characteristics of brittle fracture under general combined modes including those under bi-axial tensile loads," *Engineering Fracture Mechanics*, vol. 18, no. 6, pp. 1131–1158, 1983.

[19] H. P. Xie, Y. L. Li, R. D. Peng, and Y. Ju, "Energy analysis and criteria for structural failure of rocks," *Journal of Rock Mechanics and Geotechnical Engineering*, vol. 1, no. 1, pp. 11–20, 2009.

[20] F. Q. Gong, J. Y. Yan, and X. B. Li, "A new criterion of rock burst proneness based on the linear energy storage law and the residual elastic energy index," *Chinese Journal of Rock Mechanics and Engineering*, vol. 37, no. 9, pp. 1993–2014, 2008.

[21] Z. X. Zhang, "Kinetic energy and its applications in mining engineering," *International Journal of Mining Science and Technology*, vol. 27, no. 2, pp. 237–244, 2017.

[22] Y. Wang, W. H. Tan, D. Q. Liu, Z. Q. Hou, and C. H. Li, "On anisotropic fracture evolution and energy mechanism during marble failure under uniaxial deformation," *Rock Mechanics and Rock Engineering*, vol. 52, no. 10, pp. 3567–3583, 2019.

[23] Z. X. Zhang and F. Ouchterlony, "Energy requirement for rock breakage in laboratory experiments and engineering operations: a review," *Rock Mechanics and Rock Engineering*, vol. 55, no. 2, pp. 629–667, 2022.

[24] B. C. Yang, L. Xu, and Y. T. Duan, "Investigation into energy conversion and distribution during brittle failure of hard rock," *Bulletin of Engineering Geology and the Environment*, vol. 81, no. 3, p. 114, 2022.

[25] Q. Meng, M. Zhang, L. Han, H. Pu, and T. Nie, "Effects of acoustic emission and energy evolution of rock specimens under the uniaxial cyclic loading and unloading compression," *Rock Mechanics and Rock Engineering*, vol. 49, no. 10, pp. 3873–3886, 2016.

[26] Z. Chen, G. Su, J. Ju, and J. Jiang, "Experimental study on energy dissipation of fragments during rockburst," *Bulletin of Engineering Geology and the Environment*, vol. 78, no. 7, pp. 5369–5386, 2019.

[27] M. N. Bagde and V. Petoroš, "Fatigue and dynamic energy behaviour of rock subjected to cyclical loading," *International Journal of Rock Mechanics and Mining Sciences*, vol. 46, no. 1, pp. 200–209, 2009.

[28] F. Q. Gong, S. Luo, X. B. Li, and J. Y. Yan, "Linear energy storage and dissipation rule of red sandstone materials during the tensile failure process," *Chinese Journal of Rock Mechanics and Engineering*, vol. 37, no. 2, pp. 352–363, 2018.

[29] S. Luo and F. Q. Gong, "Linear energy storage and dissipation laws during rock fracture under three- point flexural loading," *Engineering Fracture Mechanics*, vol. 234, p. 107102, 2020.

[30] Y. Luo, F. Q. Gong, D. Q. Liu, S. Wang, and X. Si, "Experimental simulation analysis of the process and failure characteristics of spalling in D-shaped tunnels under true-triaxial loading conditions," *Tunnelling and Underground Space Technology*, vol. 90, pp. 42–61, 2019.

[31] H. P. Xie, R. D. Peng, Y. Ju, and H. W. Zhou, "On energy analysis of rock failure," *Chinese Journal of Rock Mechanics and Engineering*, vol. 24, no. 15, pp. 2603–2608, 2005.

[32] H. P. Xie, L. Y. Li, Y. Ju, R. D. Peng, and Y. M. Yang, "Energy analysis for damage and catastrophic failure of rocks," *Science China Technological Sciences*, vol. 54, no. S1, pp. 199–209, 2011.

[33] F. Q. Gong, Y. L. Wang, Z. G. Wang, J. Pan, and S. Luo, "A new criterion of coal burst proneness based on the residual elastic

energy index," *International Journal of Mining Science and Technology*, vol. 31, no. 4, pp. 553–563, 2021.

[34] F. Q. Gong, R. H. Shi, and L. Xu, "Linear energy storage and dissipation laws of concrete under uniaxial compression at different ages," *Construction and Building Materials*, vol. 318, p. 125963, 2022.

[35] F. Q. Gong, J. Y. Yan, X. B. Li, and S. Luo, "A peak-strength strain energy storage index for rock burst proneness of rock materials," *International Journal of Rock Mechanics and Mining Sciences*, vol. 117, pp. 76–89, 2019.

[36] F. Q. Gong, S. Luo, Q. Jiang, and L. Xu, "Theoretical verification of the rationality of strain energy storage index as rockburst criterion based on linear energy storage law," *Journal of Rock Mechanics and Geotechnical Engineering*, 2022.